Affiliation: Centro de Previsão de Tempo e Estudos Climáticos/Instituto Nacional de Pesquisas Espaciais, Rod. Pres. Dutra, km. 39, Cachoeira Paulista, SP, Brazil[1,2]

Additional affiliation: A.M. Obukhov Institute of Atmospheric Physics, Russian Academy of Sciences, Pyzhevski 3, Moscow, Russia[2]

Corresponding author: 55-12-31868569, pisnitch@cptec.inpe.br

The climate version of the Eta regional forecast model.

1. Evaluation of consistency between the Eta model and HadAM3P global model

I.A. Pisnichenko[1] and T.A. Tarasova[2]

25 November 2007

Abstract

The new version of Eta WS (workstation) forecast model destined for long term climate change simulation (Eta CCS) was desingned. For this, the numerous modifications and corrections have been made in the original codes of the Eta WS model as well as new program blocks were added. As a first step in the Eta CCS validation program, the Eta CCS model has been integrated over South America with the horizontal resolution of 40 km for the period of 1960-1990. It was forced at its lateral boundaries by the outputs of HadAM3P that represent simulation of modern climate with the resolution about 150 km. The run of climate Eta model was made on the supercomputer SX-6. The results of the investigation of a consistency between the output fields of the Eta model and HadAM3P are presented here. The geopotential, temperature and wind fields of both models are analysed. For the evaluation of the likeness of these two models outputs, the Fourier analysis of time series, consistency index, constituted from linear regression coefficients, time mean and space mean models' arithmetic difference and root mean square difference are used. The results of the study demonstrate that there are not significant differences in behaviour and spatial arragement of large-scale structures of the two models. Also, the regional model characteristics do not have considerable positive or negative trend during the integration in relation to the global model characteristics. From the total analysis we can affirm that in the description of large-scale climate structures by these two models are in consistency. This means that the Eta CCS model can be used for downscaling of the HadAM3P output fields.

Keywords Regional climate model, Methods of consistency evaluation

1. Introduction

The running of regional climate model (RCM) with the horizontal resolution of a few tens of kilometers over an area of interest with boundary conditions of AOGCM for the periods of 10-30 years as for the present climate as for the future projections can give additional information about the regional-scale climate and climate-change effects in this area (e.g., Dickinson et al. 1989; Giorgi and Bates 1989). Such downscaling studies related to climate change have been made already for various parts of Europe, North America, Australia, and Africa; see for example the references cited by Jones et al. (1997), Laprise et al. (2003), Giorgi et al. (2004), Duffy et al. (2006). Currently some large projects such as (PRUDENCE (Christensen et al. 2002) and NARCCAP (http://www.narccap.ucar.edu)), launched to investigate uncertainties in the RCM climate-change simulations over Europe and North America, are underway. Multiple regional climate model ensembles are used in these studies in order to minimize uncertainties in simulations with these models. The project "Climate change scenarios using PRECIS" (Jones et al. 2004) was launched by Hadley Center for Climate Prediction and Research to develop user-friendly RCM which can be easily running on personal computer for any area of the globe. The data of the atmospheric global model HadAM3P were provided by Hadley Center to CPTEC/INPE for using them as boundary condition over South America.

In order to be considered as a valid tool for dynamical downscaling of low-resolution GCM fields, a regional climate model has to satisfy some requirements (e.g., Wang et al. 2004; Castro et al. 2005; Laprise, 2006). Firstly, it is needed to show that RCM is able to reproduce more or less plausibly mean values and second moments of the large-scale fields of GCM which data are used as driving boundary conditions. This is a necessary condition indicating that nonlinear interactions of small-scale components do not strongly divert the system from the background state. It also guarantees that boundary conditions will not transform into peculiarities. This is an issue of evaluation of consistency between RCM and GCM fields. Secondly, for successful downscaling RCM must be able to add small-scale features absent in the GCM driving fields and it is necessary to show that these features agree with observations and with high-resolution GCM fields. Laprise et al. (2007) provide a summary of studies related to this item. As it was annotated in this paper the consensus on the first point is not yet reached within the RCMs community. The authors remark that it is not quite clear from analysis of RCM running if the large scales of GCM are unaffected, improved or degraded by RCMs. We also note, that a comparison of large-scale fields of RCM and GCM is mainly performed for the surface temperature and precipitation (e.g., Hudson and Jones 2002; Seth et al. 2007). Another type of comparison is presented by Castro et al. (2005) for the one month simulation of Regional Atmospheric Modeling System RAMS (Pielke et al. 1992) with the boundary conditions of the reanalysis. They did the spectral analysis of the column average total kinetic energy and the column integrated moisture flux convergence and concluded from it that RAMS does not add increased skill to the large scale available in the reanalysis.

Here we propose to use in the climate downscaling research regional climate model prepared from the NCEP Eta regional forecast model (Black 1994). Up to date the longest integrations with the Eta model have been limited to the continuous integrations for 3-5 months (Chou et al. 2000; Tarasova et al. 2006) because of the limitations in the codes of the Eta model which was developed for the weather forecast and studies. The climate version of the Eta model which permits integrations for the period of any duration were developed at the Brazilian Instituto Nacional de Pesquisas Espaciais/Centro de Previsao de Tempo e Estudos Cimaticos (INPE/CPTEC) during last years (Pisnichenko et al. 2006).

In present work we show the first results related to the development of climate version of the Eta model for climate downscaling over South America. We investigated here a consistency of the large-scale output fields of the Eta model and HadAM3P. For this, the geopotential, temperature and wind fields at various levels were analysed by using Fourier analysis of time series, consistency index, constituted from linear regression coefficients, time mean and space mean models' arithmetic difference (MAD), root mean square difference (RMSD), dispersion analysis and some others characteristics. The short description of the Eta model and of implemented modifications is given in Section 2 where the model integration procedure is also described. The newly developed version of the Eta model is hereafter termed as INPE Eta for Climate Change Simulations (INPE Eta CCS). Section 3 presents the results of the integrations with the INPE Eta CCS model over South America driven by boundary conditions from the HadAM3P for the period 1961-1991. The Eta model output fields are compared with those from HadAM3P in order to prove a consistency between the two models. Section 4 gives summary of the results and the conclusions.

2. Model and experimental design

For this work, aimed to prepare Eta model version for climate-change simulations, we initially adopted the workstation (WS) Eta modeling package (version of 2003) developed at the Science Operations Officer/Science and Training Resource Center (SOO/STRC) which is freely available at http://strc.comet.ucar. The SOO/STRC WS Eta is nearly identical to WS Eta model and operational Eta Model of 2003, both developed at NCEP. Only the run-time scripts and model files organization were changed, and additional convection cumulus scheme of Kain and Fritsch (1993) was added. The longest continuous integration with this model can be made for 1 month due to many restrictions resulting from its weather forecast destination.

2.1 Short descrip tion of NCEP Eta model

The full description of the NCEP Eta regional forecasting model is given by Mesinger et al. (1988), Janjic (1994), and Black (1994). In short, the horizontal field structure is described on a semi-staggered E grid. The eta vertical coordinate ($\eta = [(p - p_T)/(p_{sfc} - p_T)]/\eta_{srf}$, where p is a pressure, p_T and p_{sfc} are the pressure at the top and the bottom of the model boundary, and η_{srf} is a reference η) is used to reduce numerical errors over mountains in computing the pressure gradient force. The planetary boundary layer processes are described by the Mellor-Yamada level 2.5 model (Mellor and Yamada 1974). The convective precipitation scheme is of Betts and Miller (1986) modified by Janjic(1994). The shortwave and longwave radiation codes follow parameterizations of Lacis and Hansen (1974) and Fels and Schwartzkopf (1975), respectively. The land-surface scheme is of Chen et al. (1997). The grid-scale cloud cover fraction is parameterized as a function of relative humidity and cloud water (ice) mixing ratio (Xu and Randall 1996; Hong et al. 1998). Convective cloud cover fraction is parameterized as a function of precipitation rate (Slingo 1987).

2.2 Modifications in the SOO/STRC WS Eta model

The SOO/STRC WS Eta model has been installed at supercomputer NEC SX6 at CPTEC. To be able to perform long term climate integrations we have made multiple changes and corrections in the scripts and source codes of the original model as well as have written the new additional subroutines.

As it was already mentioned, the Eta model was forced at its lateral and bottom boundary by the output of HadAM3P model. The HadAM3P output data represent horizontal wind, potential temperature, specific humidity and earth surface pressure which are given on the horizontal Arakawa B-grid and at the 19 sigma-hybrid levels. These data are written in the PP-format. To use them for the Eta model boundary conditions these data have to be transformed into horizontal wind, geopotential, mixture ratio and earth surface pressure given on regular latitude-longitude grid at standard p-surface levels. For this aim, some of the pre-processing Eta model programs were modified and new program which converts the HadAM3P output data to those acceptable by the Eta model was written.

Other modifications made in the Eta model can be shortly described as following. There were re-written the SST update programs used to accept the SST and SICE data generated by HadCM3 every 15 days. The programs of the Sun's elevation angle and of calendar were modified in order to be able to integrate the Eta model for the artificial year of 360 days which is used by HadAM3P. There were developed new restart programs which allow to continue the model integration from any time moment by using the model output binary files and which can be used in multiprocessing integration. This is the useful option for a long term climate integration because of the large size of the file of boundary conditions needed for continuous integrations. Another reason for use of the restart option is the large size of the output binary files which after post-processing can be written in more economic GRIB format. All shortcomings which restrict a period of model integration were corrected including those in the post-processing subroutines.

The additional solar radiation scheme (CLIRAD-SW-M) developed by Chou and Suarez (1999) and modified by Tarasova and Fomin (2000) was implemented in the model. The results of the month integration with this scheme were analysed by Tarasova et al. (2006). The additional thermal radiation scheme of Chou et al. (2001) was also implemented. This allows to run the model with increasing concentration of $\mathrm{CO_2}$ and other trace gases needed for future climate simulation experiments. All these corrections, modifications and implementations were made taking into account that the model can be run on Linux cluster or any other multi-processors computer.

2.3 Integration with the INPE Eta CCS model

The first step in evaluation of dynamical downscaling results is the investigation of a consistency between regional model outputs and GCM data used for RCM boundary conditions. That is, we have to show that our RCM does not significantly diverge from GSM in reproducing time mean large scale patterns of circulation. It is necessary to note that the results of regional modelling, as being the solution of Cauchy-Dirichlet problem, can occur very sensitive to the errors in lateral boundary conditions (Pisnichenko et al. 2008). Notice also that these errors are always present because of the using of the linear interpolation of time-dependent boundary conditions (every 6 hours data available) into mediate time steps. In other words, we want to be sure that our model is not crucially influenced by boundary condition errors and that most stable and pronounced disturbances that are presented in GCM are reproduced by our RCM. We also expect that a low-frequency oscillation of the atmosphere are simulated by both models in a similar manner. These are necessary conditions to avoid of erroneous generation of small and middle-scale disturbances resulting from the nonlinear interactions in RCM. The verification of a consistency between the outputs of the ETA CCS RCM and driving GCM also is very advisable because of the difference between the physical parameterization packages of these two models.

For this aim we analysed the results of the Eta CCS model integration for the period 1960-1990 over South America. These data are the part of the results of current and future climate downscaling experiments covering the periods of 1960-1990 and 2071-2100, respectively. The detailed analysis of all results of these experiments is currently making by our group and will be present in further publications.

The Eta CCS model in our experiments was forced at its lateral and bottom boundary by the output of HadAM3P, which was run using SST, SICE (sea ice) and greenhouse gases and aerosol concentration as external driving from coupling model HadCM3. Data for lateral boundary conditions for the Eta CCS model were provided every 6 hours and SST and SICE data every 15 days. Linear interpolation for values on lateral boundaries, SST, and SICE was used between these periods. For the initial conditions of soil moisture and soil temperature the climate mean values were used. The spin up period of soil moisture and temperature we have accepted to be equal to 1 year. Hence, the first year of the integration was not used in the analysis.

The area of the integration was centered at $58.5°$ W longitude and $22.0°$ S latitude and covers the territory of South American continent with adjacent oceans ($55°$ S - $16°$ N, $89°$ W - $29°$ W). The model was integrated on the 211×115 horizontal grid with grid spacing of 37 km. In the vertical, 38 eta coordinate layers were used. For the modern climate integration the Betts-Miller cumulus convection parametrization scheme and the ETA model original shortwave and longwave radiation schemes were chosen.

3. Analysis of the integration results

To show a consistency between ETA CCS and HadAM3P model we have compared the geopotential height, temperature and kinetic energy fields on the earth surface and at the various p-levels (1000 mb, 700 mb, 500 mb) from these two data sources. More detailed comparison was made for the five regions shown in Figure 1: Amazonia ($12.5°$ S - $5°$ N, $75°$ W - $48.75°$ W); Nordeste (north-east of Brazil) ($15°$ S - $2.5°$ S, $45°$ W - $33.75°$ W); South of Brazil ($32.5°$ S - $22.5°$ S, $60°$ W - $48.75°$ W); Minas ($22.5°$ S - $15°$ S, $48.75°$ W - $41.25°$ W); Pantanal ($17.5°$ S - $12.5°$ S, $60°$ W - $52.5°$ W). The time averaged fields and time series of space averaged meteorological variables were analysed.

3.1 Methods of the analysis

To evaluate the consistency between the outputs of the Eta CCS regional model (hereafter RM) and HadAM3P global model (hereafter GM) we have used various measures. First, we assessed the climatological means and time averaged difference between the models, which give an opportunity to identify systematic differences between the models. Then we analysed various characteristics (root mean square difference, coeficients of linear regression, consistency index, spectra of time series), which allow to show in detail a distinction between GM and RM simulated fields. Since this work is dedicated to investigation RM abilities to reproduce mean fields of driving GM and some their statistical moments therefore the regional model fields were scaled to the global model grid. For this aim we removed the small scale component from the regional model fields applying smoothed filter. This filter is the two dimensional version of the weighted moving averages, where the weights depend linearly on the distance between the grid point of the global model and the grid points of the regional model (in which are sited the data used in smoothing procedure). The weight increases when the distance decreases. This smoothing procedure can be written as:

$$\Phi(x_i, y_j) = \sum_{r_{i,j;k} < r_0} \phi(\hat{x}_k, \hat{y}_k)\, p_k \tag{1}$$

where $\Phi(x_i, y_j)$ is a smoothed value of regional model field on global grid point, r_0 is the radius of influence which defines the circle inside which the RM field data are used for average calculation, $r_{i,j;k}$ - the distance from a (x_i, y_j) point of GM grid to k-th RM grid point $(\hat{x}_k, \hat{y}_k)$, $\phi(x_k, y_k)$ are the field value at k-th RM grid point inside the circle defined by the radius of influence, p_k is a weight for the k-th RM grid point and which is calculated as

$$p_k \;=\; \left(1 - \frac{r_{i,j;k}}{r_0}\right) / \left(\sum_{r_{i,j;k} < r_0} 1 - \frac{1}{r_0} \sum_{r_{i,j;k} < r_0} r_{i,j;k} \right). \tag{2}$$

In this formula the numerator decreases with increasing $r_{i,j;k}$ and becomes equal to zero when $r_{i,j;k}$ is equal or larger than r_0. The denominator is defined from a normalization condition, namely a sum of all p_k weights must be equal to 1.

In order to compare the models in general we analysed how they reproduce the time average fields of meteorological variables as well as the fields of standard deviation of these variables. For more detailed assessment of the consistency between the RM and GM fields we calculated the models' arithmetic difference and coefficients of linear regression using time-series of meteorological variables at each common grid point of the RM and GM model. The fields of these characteristics present useful information about a degree of consistency of the models results.

For quantitative and direct description of the consistency between the RM and GM output fields we propose to use a new characteristic which we termed a consistency index (CI). This characteristic represents some integral variant of Taylor diagram (Taylor, 2001). It is a simple functional which depends on coefficients of linear regression of GM output on RM output, standard deviations and mean values of compared series. This functional expresses the resemblance of one field to another.

We found usefulness of this characteristic in the capability to describe the similarity of two fields only by one number in the case when the space patterns are analysed. The use of unique number for describing the resemblance of two random series is of particular interest in the case when an analysis of consistency of the time evolution of the space patterns is performed. We can analyse in this case the time series of compared fields at every grid point and describe the resemblance of the time evolution of analysed fields by one field only (namely, the consistency index number at every grid point).

The numeric value of CI we define as

$$CI = \begin{cases} (1 - \dfrac{\Delta S_d}{\Delta S_n})\dfrac{\sigma_G}{\sigma_R} \quad \text{for } \dfrac{\sigma_G}{\sigma_R} \leq 1, \\ (1 - \dfrac{\Delta S_d}{\Delta S_n})\dfrac{\sigma_R}{\sigma_G} \quad \text{for } \dfrac{\sigma_G}{\sigma_R} > 1. \end{cases} \tag{3}$$

Here σ_G and σ_R are the sample standard deviation of investigated meteorological parameter of a global model series and a regional model series, respectively. The ΔS_d is the area of figure $ABOCD$ (see Figure 2) which is formed by two straight lines of linear regression and two verticals which intersects them. The straight line r is a linear regression line of the GM series on RM series. The straight line i is an ideal regression line for the identical GM and RM serieses with regression coefficients $a0 = 0$ and $a1 = 1$. The two verticals that intersect these regression lines have the coordinates of $x_R = a - s$ and $x_R = a + s$. The a is a mean value of investigated meteorological parameter of the RM series normalized on $s_0 = 1.44\sigma_R$. The s is a nondimensional value of s_0. The interval ($a - s$, $a + s$) contains 85% of members of the RM series (under the assumption that the series obeys the Gaussian distribution). ΔS_n is the area of a triangle BCE. The area of the shaded figure $ABOCD$ statistically describes a degree of resemblance of the GM and RM serieses: Smaller area corresponds to closer resemblance. The area of the triangle BCE is equal to 2 in nondimensional coordinates and describes the case when the RM and GM serieses are non-correlated and the mean value of the GM series is equal to $a-s$ (or $a+s$). The multiplier $\frac{\sigma_G}{\sigma_R}$ (or $\frac{\sigma_R}{\sigma_G}$) approximately describes the ratio of transient-eddy amplitudes reproduced by the models under comparison. Ideally, these amplitudes must be very close. The magnitude of CI is close to 1 if the GM and RM series statistically resemble one another and it is equal to zero or to negative value when there is no similarity of the serieses. When $ABOCD$ is larger than BCE the CI is less than zero what means that the resemblance of the serieses is worse than for the non-correlated serieses with the mean value of the GM series smaller (or larger) than $a + s$ ($a - s$).

Since we had to process very large amount of data, we used recurrence formulas for the calculation of averages, sample standard deviations, and coefficients of linear regression for various GM and RM serieses and wrote these characteristics to the model output every 24 hours. These characteristics for any time period can be recalculated from this running statistics. The recurrence formulas and formulas that were used for recalculation are presented in appendix A.

3.2 Assessment of the RM and GM consistency

At first we present geopotential height, temperature and kinetic energy fields averaged over the period of integration from 1961 to 1990. Figures 3 show these fields at the level of 1000 mb from the RM and GM simulations. One can see that The Eta model is able to reproduce main patterns of the HadAM3P fields. In the geopotential height field RM reproduces minimum over the northern part of the continent and maximums over subtropical Atlantic and Pacific. In the temperature fields the RM reproduces maximum over the central part of the continent and the strong north-southern gradient to the south from 30° S . The magnitude of the temperature is everywhere higher in the ETA model in comparison with GM, especially, over the central part of the continent that is probably related to the difference between the physical parameterizations of the convective scheme. RM and GM are consistent in reproducing west-north to east-south gradient in kinetic energy field. The numeric values of kinetic energy however differ slightly over most part of the continent and greater for RM. This is also related to the different physical parameterization packages in these models. The same RM and GM fields at the higher level of 700 mb bear closer spatial and quantitative resemblance (not shown). Note, that the fields similarity at 500 mb (not shown) is higher than that at 700 mb. This is a consequence of the diminishing of the impact of surface-atmosphere interaction on the higher-level atmospheric circulation. We also compared the same RM and GM fields averaged over January and July (not shown). The agreement between the fields is better in July (austral winter, when dynamics influences on the circulation more than radiation-convective physics) than in January (austral summer, when pure dynamical processes is weaker).

The fields of time standard deviation of meteorological variables provide additional information about an amplitude of their temporal fluctuations. Figure 4 presents the RM and GM standard deviation fields of geopotential height, temperature and kinetic energy at the 1000 mb level averaged over the period of integration. One can see a rather high degree of consistency between the RM and GM standard deviation fields (better than for mean fields). The standard deviation fields also bear closer resemblance for geopotential height and temperature than for kinetic energy. With the increase of altitude the difference between the RM and GM standard deviation fields is diminished for all variables (not shown).

The quantitative distinction between the two fields is usually described by the field of models' arithmetic difference (MAD) that is the difference between the fields values at each grid point. The left column of Fig. 5 shows MAD between the RM and GM geopotential height, temperature, and kinetic energy fields at 1000 mb averaged over the period of integration. One can see that the largest values of the MAD fields are over the tropical and sub-tropical parts of the Southern American continent. The significant values of MAD over the Andes are related to the errors of interpolation from the sigma-hybrid surfaces to the pressure surfaces located below the Earth's surface in the global model. With increasing of the altitude (700 mb, 500 mb) the values of MAD decrease for all fields. The MAD of these variables (geopotential height, temperature, and kinetic energy) averaged over July (January) is smaller (larger) than that averaged over all period of integration, as it was expected..

The right column of Fig. 5 presents the consistency index (CI) fields for geopotential height, temperature, and kinetic energy at the level of 1000 mb. The magnitude of CI which is close to 1 on this picture means good resemblance between the RM and GM time evolution of the variables. The CI fields resemble the fields of MAD in terms of spatial distribution. The large absolute values of MAD are correlated with small vallues of CI.But the use of non-dimensional CI allows to compare quantitatively a similarity of the fields of different meteorological variables. Thus, the CI fields in Figure 5 show that the consistency of the fields of geopotential height is higher than that of the temperature fields and the consistency of the kinetic energy field is lower than that of both geopotential height and temperature.

To compare the model outputs we also analyse a temporal variations of the geopotential height, temperature and kinetic energy values at 1000 mb 700 mb and 500 mb levels, averaged over all integration domain and over the regions shown in Figure 1. Fig. 6 presents monthly mean models' arithmetic difference and root mean square difference (RMSD) between the GM and RM time serieses for these variables averaged over the whole integration domain. For each variable the upper figure represents MAD and the lower figure shows RMSD. One can see that the magnitude of mean MAD is not high. It is about 6 m in geopotential height, less than 0.1 °K in temperature, and about 10 $m^2\,sec^{-2}$ in kinetic energy at 1000 mb. The mean RMSD values at 1000 mb are not high also. Its magnitude is about 24 m in geopotential heights, 3.4 °K in temperature, and 39 $m^2\,sec^{-2}$ in kinetic energy. Low magnitude of RMSD proves that current absolute values of MAD are not high for each moment of integration. Fig. 6 shows also that there is no permanent sistematic drift of MAD and RMSD during the integration that proves as the RM integration stability as the similar response of RM and GM on long-term forcing component. The magnitude of temporal correlation coefficient between the time serieses of the RM and GM space averaged fields is about 0.95-0.98. This means that RM principally follows the GM boundary driving. At the level of 700 mb (not shown) and 500 mb absolute values as MAD as RMSD are lower than at 1000 mb for temperature. For geopotential height and kinetic energy which are largely increased with altitude it is necessary to compare normalized on the mean value MAD and RMSD. Relative MAD and RMSD for geopotential height and kinetic energy are also diminished with altitude.

As we said it above we analysed the same time series for the next regions: Amazonia, Nordeste, South of Brazil, Minas, Pantanal. The correlation coefficients between the RM and GM time serieses as well as mean MAD and RMSD at 1000 mb and 500 mb are shown in Table 1 for all domain and for the five regions. One can see that these coefficients slightly varies from region to region. Note one case of low correlation between the kinetic energy time series at 1000 mb in Amazonia related to low magnitude of wind at the surface level in GM. Fig. 7 shows the time evolution of annual mean MAD in the geopotential height, temperature and kinetic energy fields at 1000 mb for the above mentioned regions. The magnitude of MAD for different regions varies from -10 m to +17 m for geopotential height, from -4.0°K to +0.3°K for temperature, and from -20 $m^2 sec^{-1}$ to -5 $m^2 sec^{-1}$ for kinetic energy. The amplitude of interannual variations of these meteorological variables differs from one region to another. We can see that there is no significant trend and strong fluctuations of MAD for any region. A significant mutual correlation between the MAD obtained for various regions does not exist. This indicates that local physics processes and small scaled are in general responsible for the discrepancyof models even in reproduction of large-scale, long-term component of circulation. Note that the values of MAD and the amplitudes of its interannual variations for geopotential height and temperature decrease when the altitude increases (not shown). For kinetic energy both MAD and amplitude of interannual variations increase when the altitude increases (not shown). Though the magnitude of relative MAD (for example, that divided by a mean standard deviation) for kinetic energy also decreases.

Fig. 8 presents a scattering diagram of daily linear regression coefficients values (a0, a1) which describe the regression of the GM 1000 mb geopotential height field on the same RM field (top); time evolution of these linear regression coefficients (a0 , a1) (middle) for each month of the model run; and the time evolution of consistency index (bottom). The consistency index was calculated in the same way as described above (Figure 2), but the time series were substituted by "space" series formed by variable values at all grid points. Concerning this figure we can say that in the hypothetical case, when the fields of GM and RM coincide, all points in the top figure will fall on one point with the coordinates a1=1.0 and a0=0.0. Thus we can affirm that if the points on the top figure are located near the point (a1=1, a0=0) the RM and

GM compared fields are very similar; in the case when the points are reasonably scattered but the center of mass of this distribution is close to the point (a1=1, a0=0) we can say that the fields of the models are similar in average. The time series of linear regression coefficients a0 and a1 of GM data upon RM data have large negative correlation (middle figure). In the most cases it leads to some compensation in the variations of CI shown on the bottom figure. The CI variations clearly express the year oscillation. Its mean value is about 0.84 and increases with the altitude. Its linear time trend is very small. This provides some more indication that the considered models do not diverge. Fig. 9 presents the same characteristics as shown in Fig. 8 but for the RM and GM temperature fields at 1000 mb. The scattering diagrams in this case indicates that GM is slightly warmer then RM for the regions with low temperatures and slightly colder for the regions with higher temperatures. This is in agreement with Fig. 3 which shows mean temperature fields for all period of the integration.

For more detailed analysis of the time evolution of mean values of meteorological variable fields we have calculated spectral distribution of their time series by using Fast Fourier Transform algorithm. Fig. 10 shows an example of such distribution for the time series of geopotential height, temperature and kinetic energy averaged over all integration domain. One can see that the GM and RM spectras have a high degree of similarity. The high frequency tails quasi coincide. The year and semi-year oscillations have the same amplitude. Four year cycle in geopotential height and temperature is reproduced by RM and GM quasi identically. This cycle in kinetic energy spectra is also reproduced by both models but not identically. Also the models agree in reproducing of 6-9 years minimum and of the next increase of the spectra. Quasi all synoptic and seasonal oscillation maximums coincide in the RM and GM spectras. We calculated the same spectras for above mentioned regions shown in Figure 1. The RM and GM spectras for these regions demonstrate similar coincidence as that for the whole integration domain with insignificant distinctions. Only for the Pantanal region, the spectras of GM and RM kinetic energy at 1000 mb diverge significantly. But with the increase of altitude this difference diminishes and quasi disappears at 500 mb (not shown). This resemblance of time spectra show, that though the fields of investigated meteorological variables can differ because of phase descripency in compared models, statistical behaviour of their time evolution is very similar.

4. Conclusions

This analysis of the output results of 30-year runs of the Eta regional model and its driving global model HadAM3P confirms that the models have an admissible degree of consistency despite of the difference in their physical parameterizations. The Eta model is able to reproduce main patterns of the HadAM3P mean fields of geopotential height, temperature and kinetic energy at various levels. The fields of time standard deviation of meteorological variables are also similar at all model levels. The magnitude of mean models arithmetic difference (MAD) averaged over the domain is about 6 m in geopotential height, less than 0.1 $^{\circ}$K in temperature, and about 10 $m^2\,sec^{-2}$ in kinetic energy at 1000 mb. The low magnitude of root mean square difference (RMSD) means that current absolute values of MAD are not high for each moment of the integration. There is no drift of MAD and RMSD during the integration. The magnitude of temporal correlation coefficient between the time serieses of the RM and GM space averaged fields is high (about 0.95-0.98) that means that RM follows the GM boundary driving. The spectral analysis of the RM and GM fields shows that the GM and RM spectras have a high degree of similarity. The new non-dimensional Consistency Index is proposed for evaluation of consistency between the two models. The CI fields resemble the fields of MAD in terms of spatial distribution, but allows to compare quantitatively a similarity of the fields of different meteorological variables. The comparison of the Eta CCS and HadAM3P models shows that the new climate version of the Eta model can be used in downscaling of the HadAM3P output fields.

The approach developed in this study can form the basis for quantitative assessment of regional model and its driving global model consistency. Currently, many researchers use various regional models for dynamical downscaling but a few publications exist about the quantitative assessment of the similarity between the large-scale fields of a regional model and its driving global model. Even if regional and global models have the same physical parameterization packages, the difference between the models can be related to the low time frequency and low space resolution of boundary forcing in the regional model.

In the future work we are planning to estimate an impact of tuning in RM physical parameterizations such as radiation and convection schemes on consistency of RM and GM output fields. An impact of the use of another driven global model on the RM and GM resemblance will be also estimated. We also need to evaluate the model performance for current climate by comparing regional model outputs with observations on global and regional scales. In order to estimate the impact of global model errors on the regional model outputs, the integration of the regional model driven by the reanalysis data (Kanamitsu et al. 2002) is planned.

Appendix A *Recurrence formulas*

For the evaluation of the consistency of the models we analysed very largeērieses of the meteorological data. To make the work with series faster and for economy of computer resources we used recurrence formulas for calculating running average, standard deviation and covariance, from which we can calculate any others necessary characteristics.

We accept the definition of running mean, variance and covariance respectively as

$$\bar{x}_n = \frac{1}{n}\sum_{i=1}^{n} x_i, \tag{A1}$$

$$D_n \;=\; \frac{1}{n}\sum_{i=1}^{n}(x_i - \bar{x}_n)^2, \tag{A2}$$

$$r_n \;=\; \frac{1}{n}\sum_{i=1}^{n}(x_i - \bar{x}_n)(y_i - \bar{y}_n). \tag{A3}$$

Here $\bar{x}_n$, D_n, and r_n are the sample mean, the sample variance, and the sample covariance for serieses containing n terms, x_i, y_i are the i-th term of series. The recurrence formula for a sample mean is obvious

$$\bar{x}_n \;=\; \frac{n-1}{n}\bar{x}_{n-1} + \frac{1}{n}x_n. \tag{A4}$$

Below we derive the recurrence formula for a sample covariance. The analogous formula for a sample variance is obtained after replacing y_i, $\bar{y}_n$ by x_i, $\bar{x}_n$.

Let us rewrite formula (A3) using (A4) in following manner

$$r_n \;=\; \frac{n-1}{n}\cdot\frac{1}{n-1}\sum_{i=1}^{n-1}(x_i - \frac{n-1}{n}\bar{x}_{n-1} - \frac{1}{n}x_n)(y_i - \frac{n-1}{n}\bar{y}_{n-1} - \frac{1}{n}y_n)+$$
$$+\frac{1}{n}(x_n - \bar{x}_n)(y_n - \bar{y}_n)$$

Now we group the members of this formula to select the part that is equal to the covariance on previous $(n-1)$ step

$$r_n \;=\; \frac{n-1}{n}\cdot\frac{1}{n-1}\sum_{i=1}^{n-1}(x_i - \bar{x}_{n-1})(y_i - \bar{y}_{n-1}) + \frac{1}{n}(\bar{y}_{n-1} - y_n)\cdot\frac{n-1}{n}\cdot\frac{1}{n-1}\sum_{i=1}^{n-1}(x_i -$$
$$-\bar{x}_{n-1}) + \frac{1}{n}(\bar{x}_{n-1} - x_n)\frac{n-1}{n}\cdot\frac{1}{n-1}\sum_{i=1}^{n-1}(y_i - \bar{y}_{n-1}) + \frac{1}{n}(\bar{x}_{n-1} - x_n)\cdot\frac{1}{n}(\bar{y}_{n-1} - y_n)\cdot$$
$$\cdot\frac{n-1}{n} + \frac{1}{n}(x_n - \bar{x}_n)(y_n - \bar{y}_n).$$

Taking into account that the terms $\frac{1}{n-1}\sum_{i=1}^{n-1}(x_i - \bar{x}_{n-1})$ and $\frac{1}{n-1}\sum_{i=1}^{n-1}(y_i - \bar{y}_{n-1})$ are equal to zero and using again formula (A4) we obtain

$$r_n \;=\; \frac{n-1}{n}r_{n-1} + \frac{n-1}{n^2}(\bar{x}_{n-1} - x_n)(\bar{y}_{n-1} - y_n). \tag{A5}$$

Finally we show how to recalculate these running values for any time interval. Let $\bar{x}_m$ be the mean value for series from the first m elements of x_i and let $m < n$. Denote $\bar{x}_{m:n}$ the mean value of x_i for the series $x_{m+1}, x_{m+2}, ...x_n$ as

$$\bar{x}_{m:n} = \frac{1}{n-m}\sum_{i=m+1}^{n} x_i,$$

It is easy to obtain that

$$\bar{x}_{m:n} = \frac{1}{n-m}(n\bar{x}_n - m\bar{x}_m). \tag{A6}$$

Now, let us derive formula for calculating the covariance for interval $(m+1, n)$ using the meanings for covariance and average for intervals $(1, m)$ and $(1, n)$.

$$n\bar{r}_n - m\bar{r}_m = \sum_{i=1}^{n}(x_i y_i) - n\bar{x}_n\bar{y}_n - \sum_{i=1}^{m}(x_i y_i) + m\bar{x}_m\bar{y}_m \tag{A7}$$

Taking into account that

$$(n-m)\bar{r}_{m:n} = \sum_{i=m+1}^{n}(x_i y_i) - (n-m)\bar{x}_{m:n}\bar{y}_{m:n}, \tag{A8}$$

we rewrite (A7) as

$$n\bar{r}_n - m\bar{r}_m = (n-m)\bar{r}_{m:n} - n\bar{x}_n\bar{y}_n + m\bar{x}_m\bar{y}_m + (n-m)\bar{x}_{m:n}\bar{y}_{m:n}. \tag{A9}$$

Lastly, substituting the $\bar{x}_{m:n}, \bar{y}_{m:n}$ from formula (A6) and making routine transformations we obtain the desired formula

$$\bar{r}_{m:n} = \frac{1}{n-m}(n\bar{r}_n - m\bar{r}_m) - \frac{mn}{(n-m)^2}(\bar{x}_n - \bar{x}_m)(\bar{y}_n - \bar{y}_m). \tag{A10}$$

Acknowledgments. I.A. Pisnichenko was supported by Global Opportunity Fund (GOF) from UK Foreign Commonwealth Office, T.A. Tarasova was sponsored by INPE/CPTEC as part of an international agreement with the NEC Corporation. The authors thank their colleagues from CPTEC/INPE C. Nobre and J. Marengo for their administrative contributions that made it possible for us to perform this work. The authors also thank Hadley Center for presenting HadAM3P data.

References

Betts AK, and Miller MT (1986) A new convective adjustment scheme. Part II: Single column tests GATE wave, BOMEX, and Arctic air-mass data. Quart J Roy Met Soc 112: 693-703

Black TL (1994) NMC notes: the new NMC mesoscale Eta model: description and forecast examples. Wea Forecasting 9:256-278

Castro CL, Pielke Sr RA, and Leoncini G (2005) Dynamical downscaling: Assessment of value retained and adding using the Regional Atmosphering Modeling System (RAMS). J Geophys Res 110(D05108) doi: 10.1029/2004JD004721

Chou M-D, and Suarez MJ (1999) A solar radiation parameterization (CLIRAD-SW) for atmospheric studies. Preprint NASA/Goddard Space Flight Center, Greenbelt, Maryland, 38 pp

Chou M-D, Suarez MJ, Liang X-Z, and Yan M M-H (2001) A thermal infrared radiation parameterization for atmospheric Studies. Preprint NASA/Goddard Space Flight Center, Greenbelt, Maryland, 55 pp

Chen FK, Janjic Z, and Mitchel K, (1997) Impact of the atmospheric surface-layer parameterizations in the new land-surface scheme of the NCEP mesoscale Eta model. Bound-Layer Meteor 85: 391-421

Christensen JH, Carter T, and Giorgi F (2002) PRUDENCE employs new methods to assess European climate change. EOS Trans Amer Geophys Union 82:147

Chou SC, Nunes AMB, and Cavalcanti IFA (2000) Extended forecast over South America using the regional Eta model. J Geophys Res 105:10147-10160.

Duffy PB, Arritt RW, Coquard J, Gutowski W, Han J, Iorio J, Kim J, Leung L-R, Roads J, Zeledon E (2006) Simulations of present and future climates in the western United States with four nested regional climate models. J Clim 19:873-895

Dickinson RE, Errico RM, Giorgi F, and Bates GT (1989) A regional climate model for the western

United States. Clim Change 15:383-422

Fels SB, and Schwartzkopf MD (1975) The simplified exchange approximation: A new method for radiative transfer calculations. J Atmos Sci 32:1475-1466

Fernandez JPR, Franchito SH, and Rao VB (2006) Simulation of the summer circulation over South America by two regional climate models. Part I: Mean climatology. Theor Appl Climatol 86:247-260

Giorgi F, and Bates GT (1989) The climatological skill of a regional model over complex terrain. Mon Wea Rev 117:2325-2347

Giorgi F, Bi X, Pal JS (2004) Mean, interannual variability and trends in a regional climate change experiment over Europe. I. Present-day climate (1961-1990). Clim Dyn 22:733-756 doi: 10.1007/s00382-004-0409-x

Hong S-Y, Yuang H-M, and Zhao Q (1998) Implementing of prognostic cloud scheme for a regional spectral model. Mon Wea Rev 126:2621-2639

Hudson DA, and Jones RD (2002) Regional climate model simulations of present-day and future climates of Southern Africa. Hadley Centre for Climate Prediction and Research, Met Office, Bracknell, UK

Janjic ZI (1994) The step-mountain eta coordinate model: further development of the convection, viscous sublayer, and turbulence closure schemes. Mon Wea Rev 122:927-945

Jones RG, Murphy JM, Noguer M, Keen AB (1997) Simulation of climate change over Europe using a nested regional-climate model. II: Comparison of driving and regional model responses to a doubling of carbon dioxide. Quart J Roy Met Soc 123:265-292

Jones RG, Noguer M, Hassel DC, Hudson D, Wilson SS, Jenkins GJ, and Mitchell JFB (2004) Generating high resolution climate change scenarios using PRECIS. Met Office, Hadley Center, Exeter, UK, 40 pp

Kanamitsu M, Ebisuzaki W, Woollen J, Yang S-K, Hnilo JJ, Fiorino M, and Potter GL (2002) NCEP-DOE AMIP-II Reanalysis (R-2). Bull Amer Meteor Soc 83:1631-1643

Kain JS, and Fritsch JM (1993) A one-dimensional entraining detraining plume model and its applications in convective parameterization. J Atmos Sci 23:2784-2802

Lacis AA, and Hansen JE (1974) A parameterization for the absorption of solar radiation in the Earth's atmosphere. J Atmos Sci 31:118-133

Laprise R, Caya D, Frigon A, Paquin D (2003) Current and perturbed climate as simulated by the second-generation Canadian Regional Climate Model (CRCM-II) over north-western North America. Clim Dyn 21:405-421 doi: 10.1007/s00382-003-0342-4

Laprise R (2006) Regional climate modelling. J Comput Phys doi: 10.1016/j.jcp.2006.10.024

Laprise R, de Elia R, Caya D et al (2007) Challenging some tenets of regional climate modelling.

Mellor GL, and Yamada T (1974) A hierarchy of turbulence closure models for boundary layers. J Atmos Sci 31:1791-1806.

Mesinger F, Janjic ZI, Nickovic S, Gavrilov D, and Deaven DG (1988) The step-mountain coordinate: model description and performance for cases of Alpine lee cyclogenesis and for a case of Appalachian redevelopment. Mon Wea Rev 116:1493-1518

Pielke Sr RA et al (1992) A comprehensive meteorological modeling system - RAMS. Meteorol Atmos Phys 49:69-91

Pisnichenko IA, Tarasova TA, Fernandez JPR, and Marengo J (2006) Validation of the Eta WS regional climate model driven by boundary conditions from the HADAM3P over South America. Proceedings of 8 ICSHMO, Foz do Iguacu, Brazil, April 24-28, INPE, 595-597

Pisnichenko FI, Pisnichenko IA, Martinez JM, and Santos SA (2008) Continuing dynamic assimilation of the inner region data in hydrodynamics modelling: Optimization approach. `http://arxiv.org/pdf/0801.1683v1`

Seth A, Rauscher SA, Camargo SJ (2007) RegCM3 regional climatologies for South America using reanalysis and ECHAM global model driving fields. Clim Dyn 28:461-480 doi: 10.1007/s00382-006-0191-z

Slingo JM (1987) The development of a cloud prediction model for the ECMWF model. Quart J Royal Met Soc 113:899-927

Tarasova TA, and Fomin BA (2000) Solar radiation absorption due to water vapor: Advanced broad-band parameterizations. J Appl Meteor 39:1947-1951

Taylor KE (2001) Summarizing multiple aspects of model performance in single diagram: J Geophys Res 106:7183-7192

Vernekar AD, Kirtman BP, Fennessy MJ (2003) Low-level jets and their effects on the South American summer climate by the NCEP Eta Model. J Clim 16:297-311

Tarasova TA, Fernandez JPR, Pisnichenko IA, Marengo JA, Ceballos JC, and Bottino MJ (2006) Impact of new solar radiation parameterization in the Eta Model on the simulation of summer climate over South America. J Appl Meteor Climatol 44:318-333

Wang Y, Leung LR, McGregor JL, Lee D-K, Wang W-C, Ding Y, and Kimura F (2004) Regional climate modeling: progress, challenges, and prospects. J Meteor Soc Jpn 82:1599-1628

Xu K-M, and Randall DA (1996) A semi empirical cloudiness parameterization for use in climate models. J Atmos Sci 53:3084-3102

Figure captions

Figure 1. The regions over South America selected for the analysis: Amazonia (1), Nordeste (2), Sul Brasil (3), Minas (4), Pantanal (5).

Figure 2. Definition of consistency index by using the coefficients of linear regression of HadAM3P field on Eta CCS model field.

Figure 3. Mean (1961-1990) fields of geopotential height (m), temperature (°K), and kinetic energy ($m^2\,sec^{-2}$) at 1000 mb, provided by HadAM3P (left) and Eta CCS model (right) simulations.

Figure 4. Mean (1961-1990) standard deviation fields of geopotential height (m), temperature (°K), and kinetic energy ($m^2\,sec^{-2}$) at 1000 mb, provided by HadAM3P (left) and Eta CCS model (right) simulations.

Figure 5. Mean (1961-1990) fields of MAD (left), calculated for HadAM3P and Eta CCS model fields of geopotential height (m), temperature (°K), and kinetic energy ($m^2\,sec^{-2}$) at 1000 mb, and consistency index between HadAM3P and Eta CCS model(right), calculated for the same fields.

Figure 6. Time series of mean (over the integration domain) MAD and RMSD, calculated for HadAM3P and Eta CCS model fields of geopotential height (m), temperature (°K), and kinetic energy ($m^2\,sec^{-2}$) at 1000 mb (left) and 500 mb (right).

Figure 7. Time series of mean (over the regions shown in Figure 1) MAD, calculated for HadAM3P and Eta CCS model fields of geopotential height, G (m), temperature, T (°K), and kinetic energy, KE ($m^2\,sec^{-2}$) at 1000 mb.

Figure 8. Scattering diagram of daily coefficients (a0, a1) of linear regression of HadAM3P field on Eta CCS model field of geopotential height at 1000 mb calculated over the all integration domain (top); time series of regression coefficients (a0, a1) (middle), time series of consistency

index for these models (bottom).

Figure 9. The same as in Figure 12 but for temperature at 1000 mb

Figure 10. Time spectra of mean (over the integration domain) geopotential height (top), temperature (middle), and kinetic energy (bottom) at 1000 mb, provided by HadAM3P (solid) and Eta CCS model (dot-dashed) simulations.

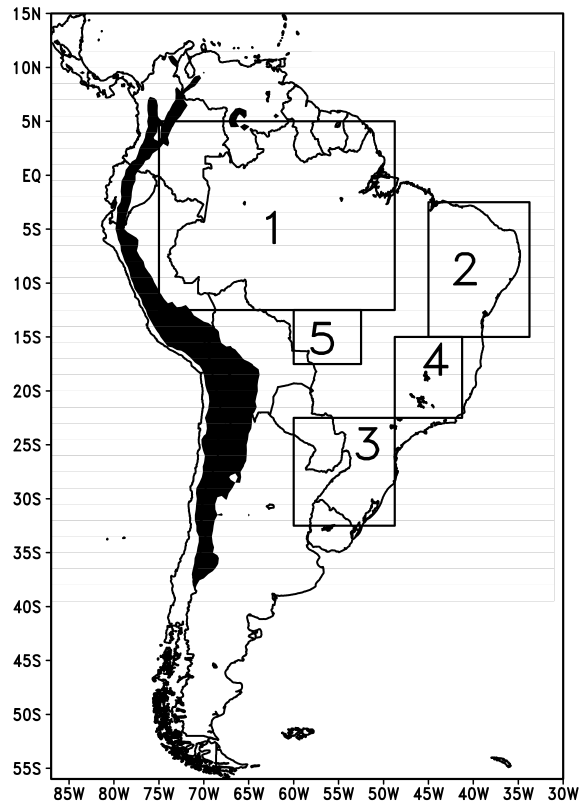

Figure 1: The regions over South America selected for the analysis: Amazonia (1), Nordeste (2), Sul Brasil (3), Minas (4), Pantanal (5).

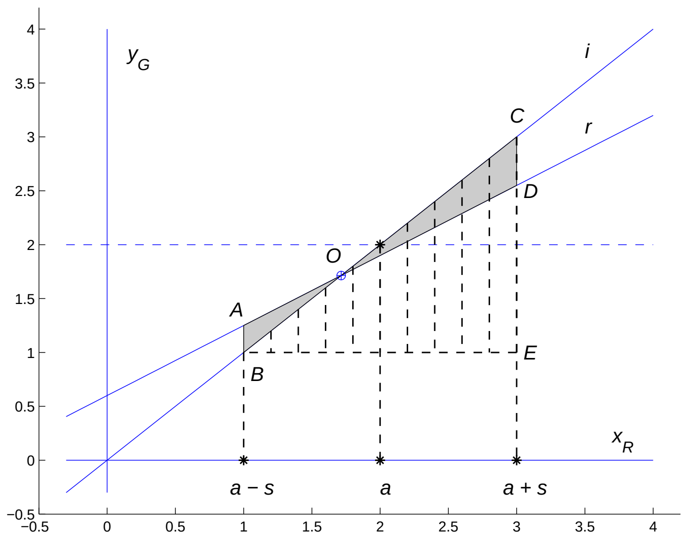

Figure 2: Definition of consistency index by using the coefficients of linear regression of HadAM3P field on Eta CCS model field.

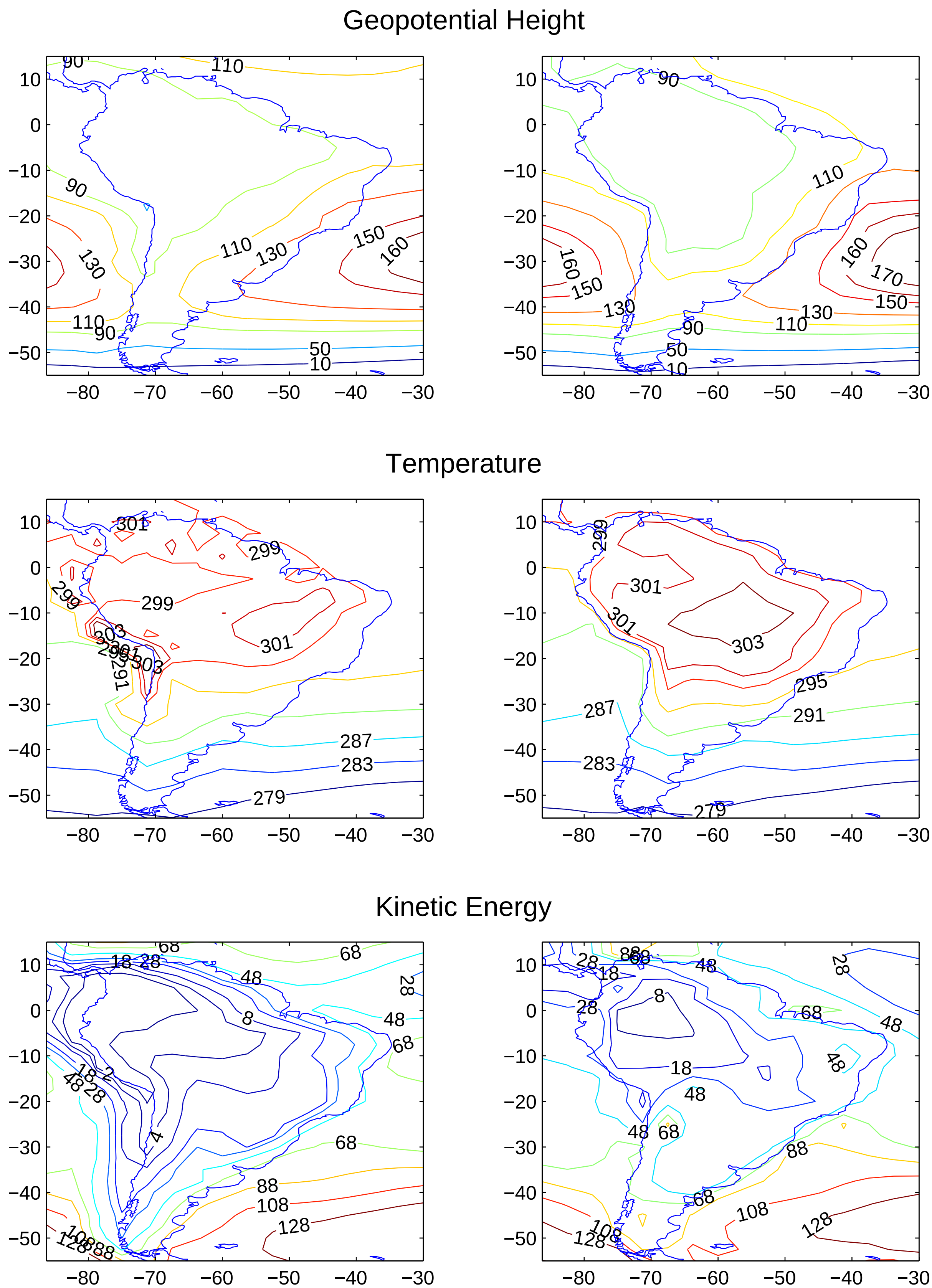

Figure 3: Mean (1961-1990) fields of geopotential height(m), temperature (°K), and kinetic energy (m^2 sec^{-2}) at 1000 mb, provided by HadAM3P (left) and Eta CCS model (right) simulations.

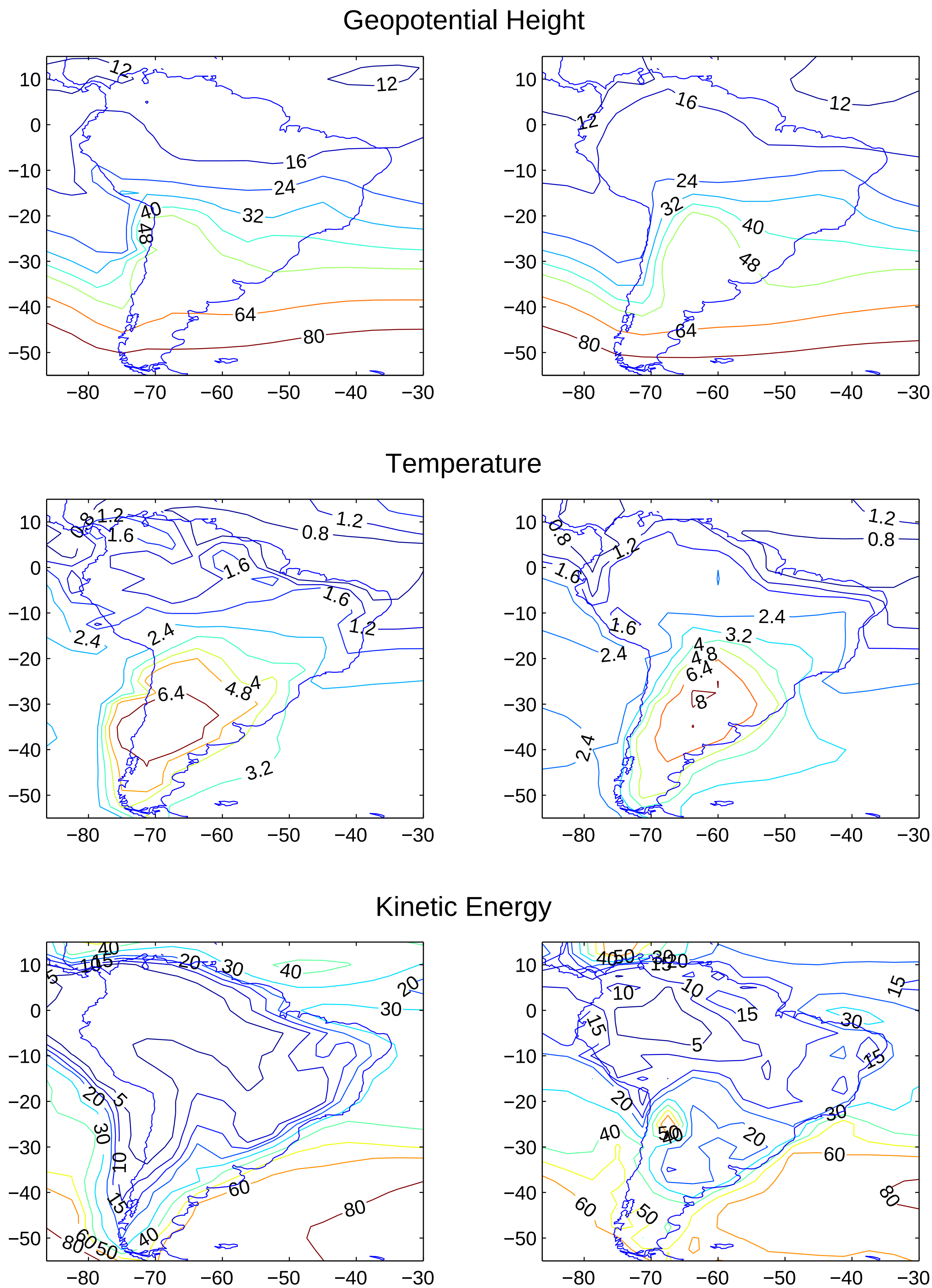

Figure 4: Mean (1961-1990) standard deviation fields of geopotential height (m), temperature (°K), and kinetic energy ($m^2\,sec^{-2}$) at 1000 mb, provided by HadAM3P (left) and Eta CCS model (right) simulations.

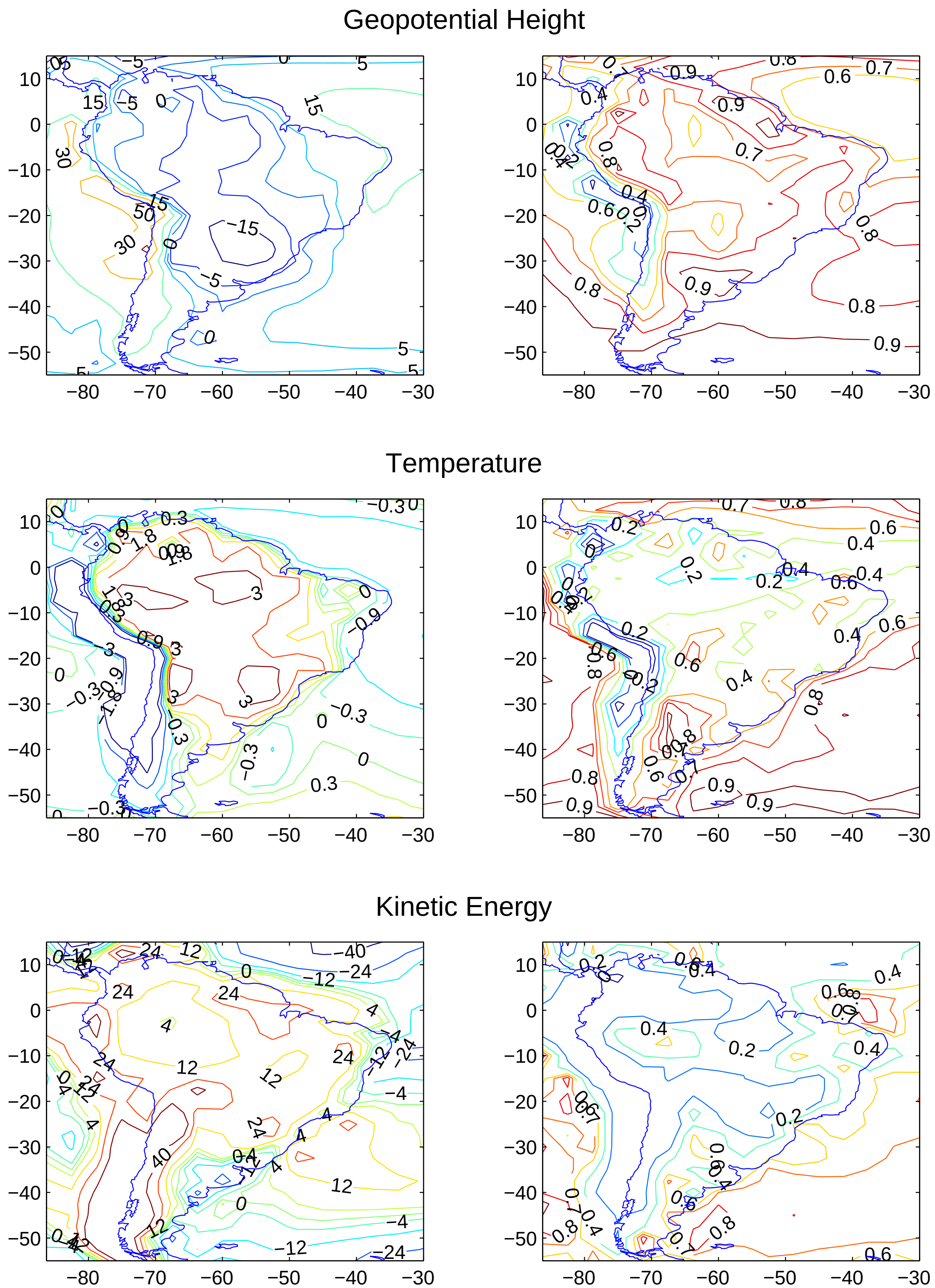

Figure 5: Mean (1961-1990) fields of MAD (left), calculated for HadAM3P and Eta CCS model fields of geopotential height (m), temperature (°K), and kinetic energy ($m^2\,sec^{-2}$) at 1000 mb, and consistency index between HadAM3P and Eta CCS model(right), calculated for the same fields.

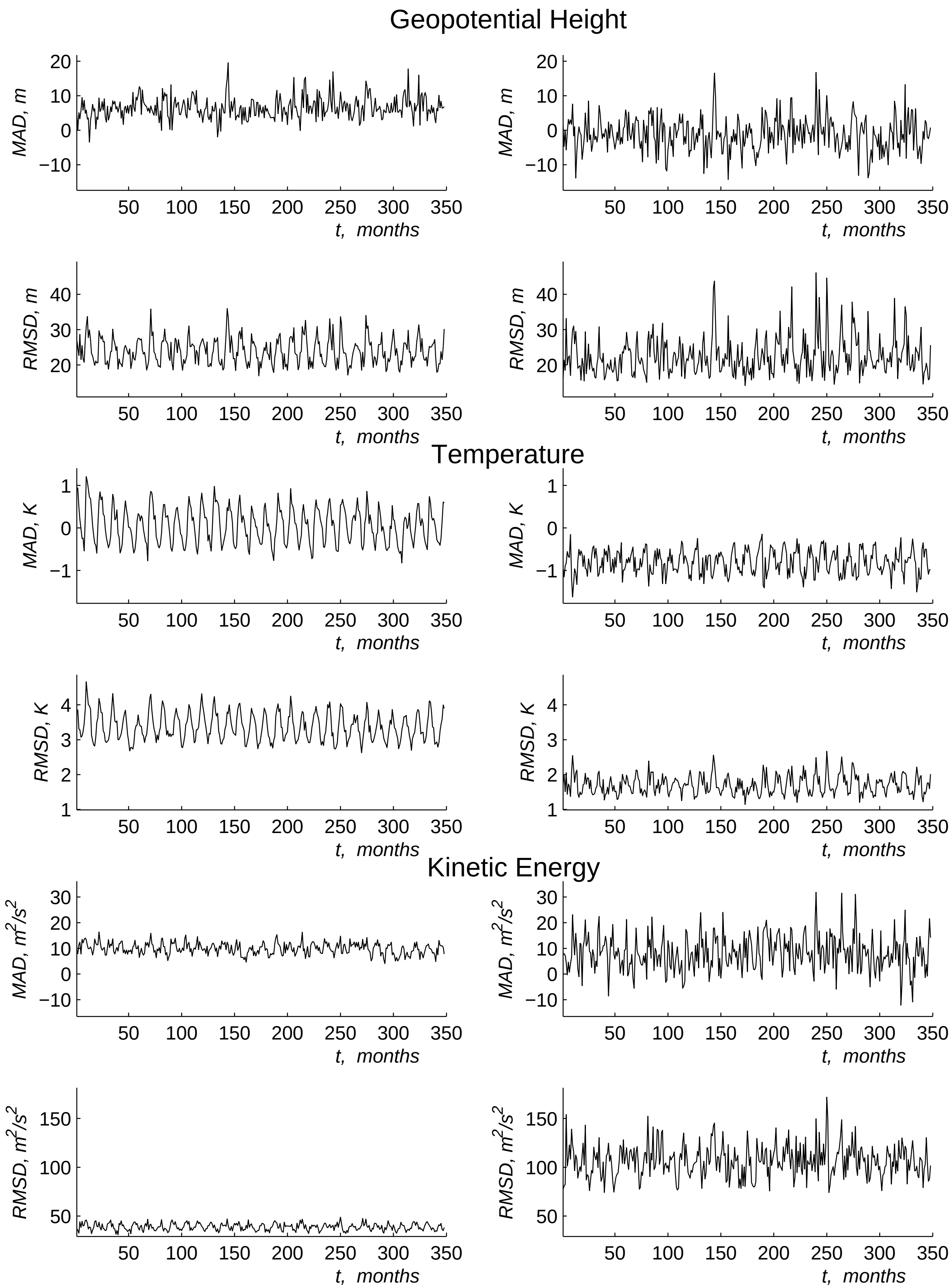

Figure 6: Time series of mean (over the integration domain) MAD and RMSD, calculated for HadAM3P and Eta CCS model fields of geopotential height (m), temperature (°K), and kinetic energy ($m^2\,sec^{-2}$) at 1000 mb (left) and 500 mb (right).

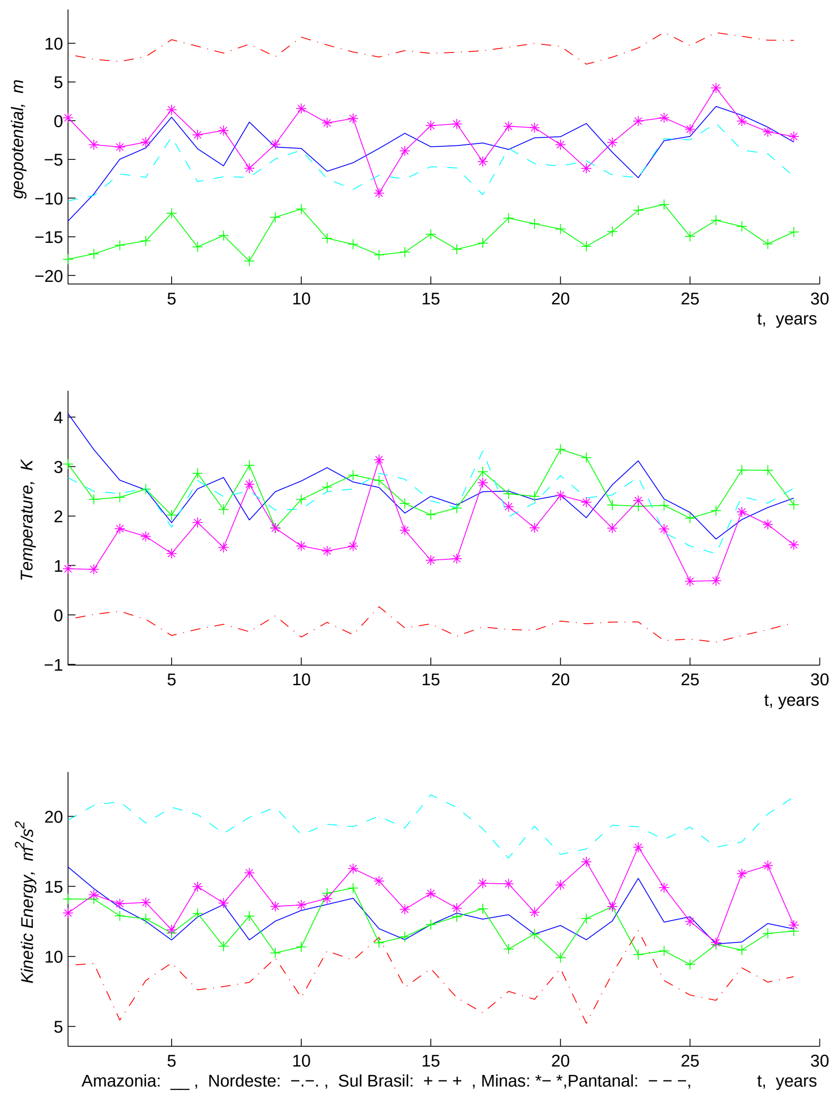

Figure 7: Time series of mean (over the regions shown in Figure 1) MAD, calculated for HadAM3P and Eta CCS model fields of geopotential height, G (m), temperature, T (°K), and kinetic energy, KE (m^2 sec^{-2}) at 1000 mb.

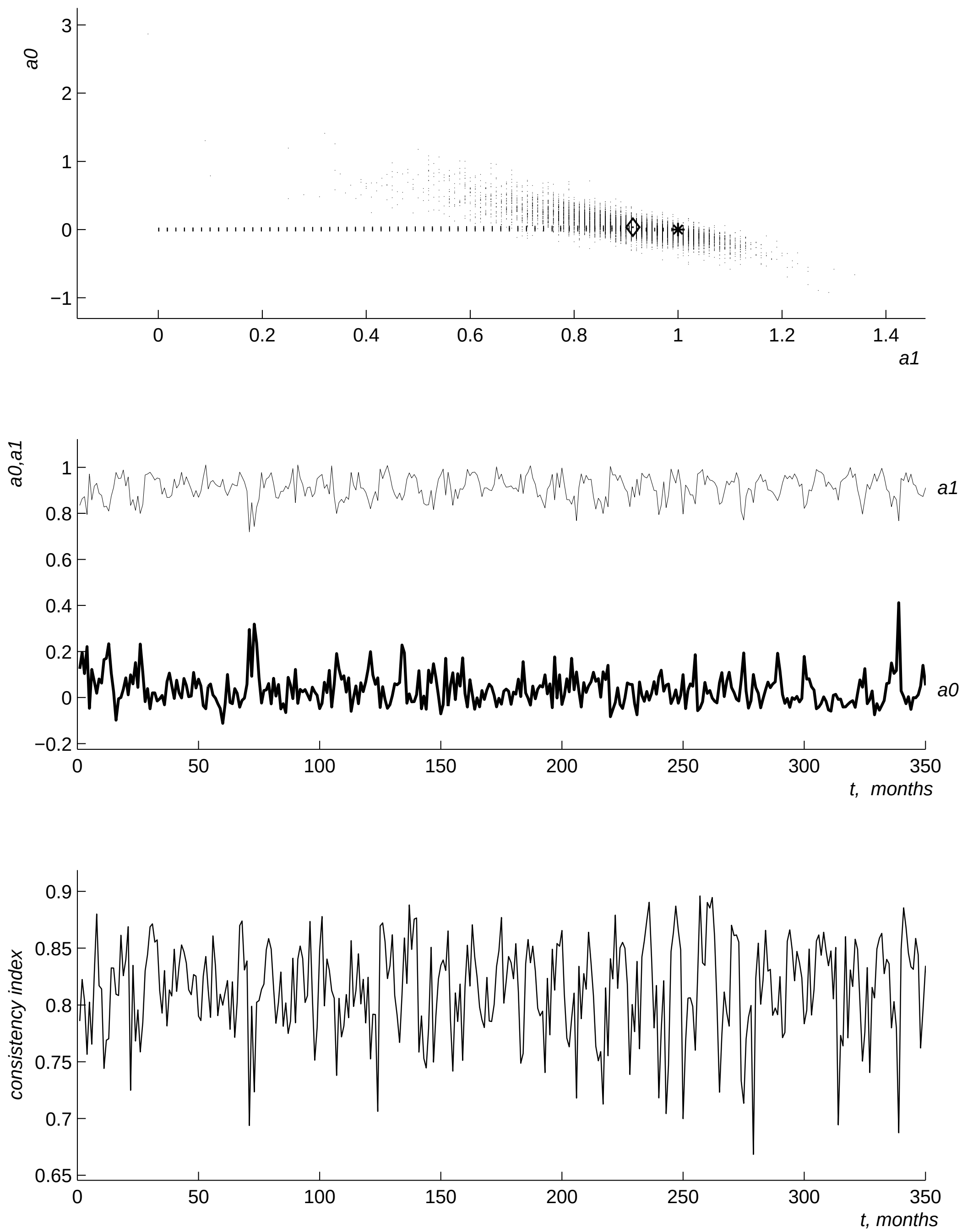

Figure 8: Scattering diagram of daily coefficients (a0, a1) of linear regression of HadAM3P field on Eta CCS model field of geopotential height at 1000 mb calculated over the all integration domain (top); time series of regression coefficients (a0, a1) (middle), time series of consistency index for these models (bottom).

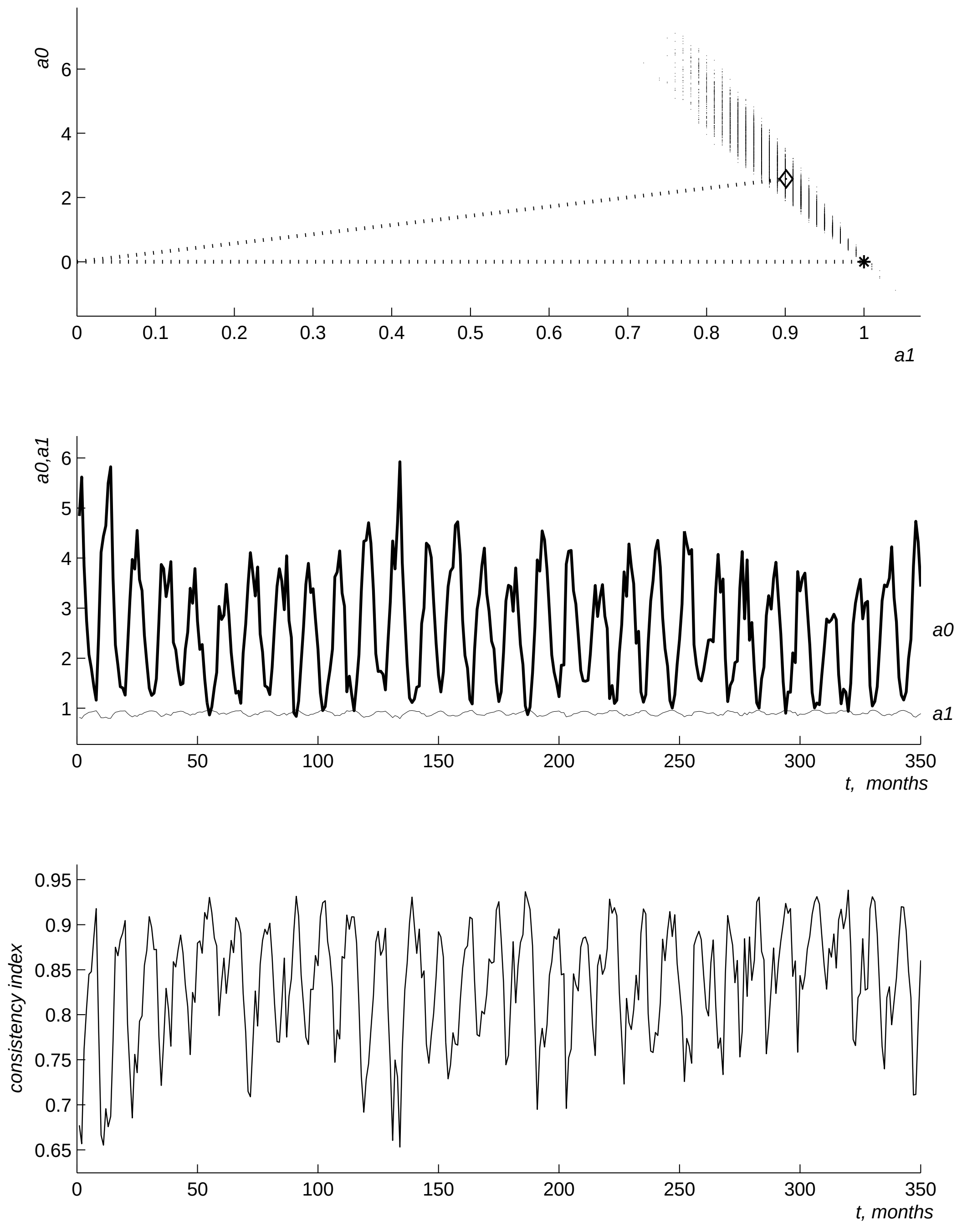

Figure 9: The same as in Figure 12 but for temperature at 1000 mb.

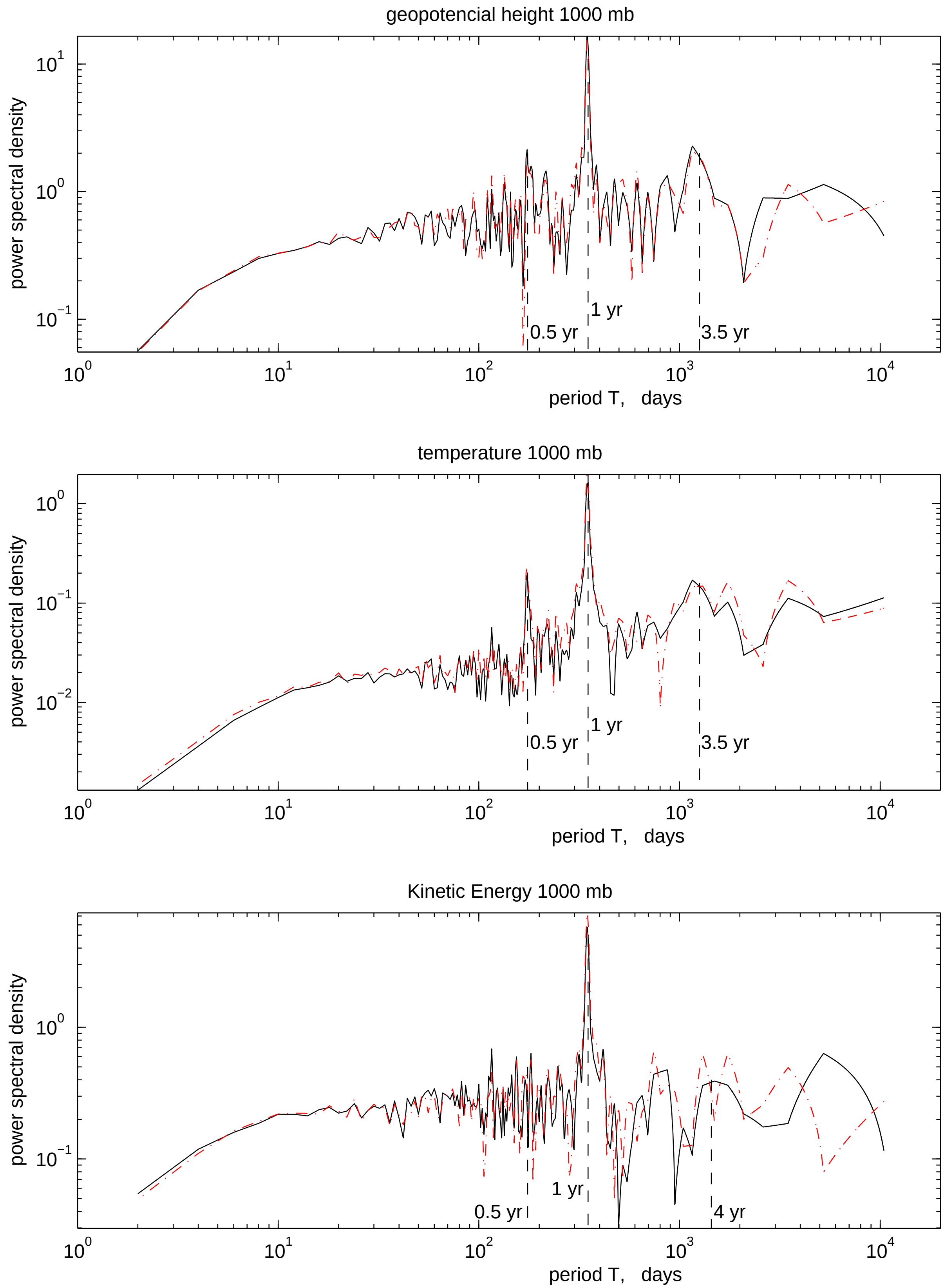

Figure 10: Time spectra of mean (over the integration domain) geopotential height (top), temperature(middle), and kinetic energy (bottom) at 1000 mb, provided by HadAM3P (solid) and Eta CCS model (dot-dashed) simulations.

Table 1. Mean correlation coefficient (r), mean MAD , and mean RMSD between the regional and global models time series of geopotential height (G), temperature (T), and kinetic energy (KE) at 1000 mb and 500 mb, averaged over the integration domain (D) and over the 5 regions shown in Figure 1.

	G			T			KE		
Region	r	MAD	RMSD	r	MAD	RMSD	r	MAD	RMSD
				Pressure level of 1000 mb					
D	0.98	6	24	0.98	0.1	3.4	0.95	10	39
1	0.95	-3	9	0.78	2.5	3.0	0.51	13	17
2	0.97	9	13	0.92	-0.2	1.7	0.9	8	23
3	0.97	-15	25	0.96	2.5	4.2	0.83	12	27
4	0.95	-2	17	0.72	1.7	3.0	0.69	14	20
5	0.97	-6	14	0.64	2.4	3.5	0.79	20	22
				Pressure level of 500 mb					
D	0.97	-1	23	0.99	-0.8	1.7	0.98	8	11
1	0.97	-2	6	0.81	-1.0	1.4	0.81	13	42
2	0.94	-1	8	0.81	-0.9	1.5	0.61	12	40
3	0.89	3	26	0.97	-1.0	1.8	0.93	7	111
4	0.74	2	16	0.88	-1.1	1.6	0.86	9	55
5	0.77	-1	10	0.79	-1.6	1.8	0.84	11	36